

# Stochastic Acceleration of $^3\text{He}$ and $^4\text{He}$ in Solar Flares by Parallel Propagating Plasma Waves: General Results

Siming Liu<sup>1</sup>, Vahé Petrosian<sup>1,2</sup>, and Glenn M. Mason<sup>3</sup>

## ABSTRACT

In this work we study the acceleration in solar flares of  $^3\text{He}$  and  $^4\text{He}$  from a thermal background by parallel propagating plasma waves with a general broken power-law spectrum that takes into account the turbulence generation processes at large scales and the thermal damping effects at small scales. The exact dispersion relation for a cold plasma is used to describe the relevant wave modes. In the nonrelativistic regime of interest here the charged particle acceleration is dominated by resonant interactions with high frequency waves, and the pitch angle diffusion rate is usually smaller than the momentum diffusion rate below a few MeV nucleon<sup>-1</sup>. In the absence of other more efficient scattering agents, this may give rise to an anisotropic particle distribution. Because low-energy  $\alpha$ -particles only interact with small scale waves in the  $^4\text{He}$ -cyclotron branch, where the wave frequencies are below the  $\alpha$ -particle gyro-frequency, their pitch angle averaged acceleration time is at least one order of magnitude longer than that of  $^3\text{He}$  ions, which mostly resonate with relatively higher frequency waves in the proton-cyclotron (PC) branch. The  $\alpha$ -particle acceleration rate starts to approach that of  $^3\text{He}$  beyond a few tens of keV nucleon<sup>-1</sup>, where  $\alpha$ -particles can also interact with long wavelength waves in the PC branch. However, the  $^4\text{He}$  acceleration rate is always smaller than that of  $^3\text{He}$ . Consequently, the acceleration of  $^4\text{He}$  is suppressed significantly at low energies, and the spectrum of the accelerated  $\alpha$ -particles is always softer than that of  $^3\text{He}$ . The effects of thermal damping further magnify this suppression. On the other hand, the length scale of waves in the PC branch at generation (the longest scale) mostly affects the high-energy cutoffs of the accelerated particle spectra. These favorable conditions for  $^3\text{He}$

---

<sup>1</sup>Center for Space Science and Astrophysics, Department of Physics, Stanford University, Stanford, CA 94305; liusm@stanford.edu

<sup>2</sup>Department of Physics and Applied Physics, Stanford University, Stanford, CA 94305; vahe@astronomy.stanford.edu

<sup>3</sup>Department of Physics and Institute for Physical Sciences and Technology, University of Maryland, College Park, MD 20742-4111; glenn.mason@umail.umd.edu

acceleration diminish in strongly magnetized plasmas and/or for strong turbulence. The model gives reasonable account of the observed low-energy  $^3\text{He}$  and  $^4\text{He}$  fluxes and spectra in the impulsive solar energetic particle events observed with the *Advanced Composition Explorer*. Other acceleration processes and/or stochastic acceleration by other wave modes seem to be required to explain the occasionally observed decrease of  $^3\text{He}$  to  $^4\text{He}$  ratio at energies beyond a few MeV nucleon $^{-1}$ .

*Subject headings:* acceleration of particles — plasma — Sun: abundances — Sun: flares — turbulence

## 1. INTRODUCTION

Stochastic acceleration (SA) of particles by plasma waves or turbulence (PWT), a second order Fermi acceleration process, plays an important role in understanding the energy release processes and the consequent plasma heating and particle acceleration in solar flares (e.g., Ramaty 1979; Möbius et al. 1980, 1982; Miller et al. 1997; Petrosian & Liu 2004, hereafter PL04). This theory was applied to the acceleration of nonthermal electrons (Miller & Ramaty 1987; Hamilton & Petrosian 1992; Park, Petrosian & Schwartz 1997; Petrosian & Donaghy 1999), which are responsible for the microwave and hard X-ray emissions and for type III radio bursts during the impulsive phase of solar flares. In this respect it has achieved some degree of success (see PL04). It has also been advocated for production of nonthermal electrons and ions observed near the Earth in association with solar flares (Reames, von Rosenvinge & Lin 1985; Mason et al. 1989; Van Hollebeke, McDonald & Meyer 1990; Bieber et al. 1994). The accelerated ions show charge-to-mass ratio dependent enhancements relative to the photospheric values, which are readily explained in the context of SA (Miller 2003; Hurford et al. 1975; Reames, Meyer & von Rosenvinge 1994; Mason et al. 1986, 2002, 2004; Reames & Ng 2004). In a few gamma-ray flares, where gamma-ray line emissions due to ion nuclear interactions are clearly observed, there is also evidence for an anomalous abundance pattern of the accelerated ions (Share & Murphy 1998; Hua, Ramaty & Lingenfelter 1989). The competing models of diffusive shock acceleration and/or direct acceleration by parallel (to magnetic fields) electric fields have not been subjected to quantitative tests. In addition maintaining large electric fields appears to be problematical (see, however, Holman 1985), and there is no convincing evidence for the presence of low coronal shocks for the impulsive flares.

The most critical challenge to these models including the SA model arises from the extreme enhancement of  $^3\text{He}$  observed in some scatter free impulsive events (Hsieh & Simpson

1970; Serlemitsos & Balasubrahmanyam 1975; Mason, Dwyer & Mazur 2000). All models proposed for this are based on either resonant plasma heating or resonant particle acceleration (Fisk 1978; Temerin & Roth 1992; Miller & Viñas 1993; Zhang 1999; Paesold, Kallenbach & Benz 2003). We recently carried out a quantitative study and showed that the SA of  $^3\text{He}$  and  $^4\text{He}$  by parallel propagating plasma waves can account for the  $^3\text{He}$  enhancement, its varied range, and the spectral shape (Liu, Petrosian & Mason 2004, hereafter LPM04). The primary feature of our new finding, which comes from our use of the exact dispersion relation, is that the acceleration of  $^4\text{He}$  from a low-energy thermal background is suppressed due to its lack of resonance with multiple-waves, a result very similar to the suppression of proton acceleration relative to the electron acceleration (Schlickeiser 1989; PL04).

Earlier studies of SA of low-energy thermal background electrons and protons revealed an acceleration rate larger than the scattering rate (Pryadko & Petrosian 1997; PL04). We show here that, for coronal conditions, this is also true for the SA of  $^3\text{He}$  and  $^4\text{He}$ . Consequently, in impulsive events SA by PWT at low energies (determined by the acceleration rate) is more efficient than the acceleration by diffusive shocks, whose rate of acceleration is proportional to the scattering rate. In addition, recent observations of gradual events, which may involve acceleration by interplanetary shocks, suggest that the source population is pre-accelerated by a distinct acceleration process operating in impulsive or gradual flares (Mason, Mazur & Dwyer 1999; Desai et al. 2001, 2003, 2004). SA may very well be the agent for this acceleration as well.

In this paper we explore more realistic models and quantify the dependence of  $^3\text{He}$  enhancement on basic model parameters. In the next section we discuss the basic features of resonant wave-particle interaction. After showing that the scattering rate is usually lower than the acceleration rate at low energies, we calculate the pitch angle averaged acceleration timescales of  $^3\text{He}$  and  $^4\text{He}$  under different plasma conditions and for different turbulence spectra, taking into account the uncertainties associated with the generation of turbulence, its cascade and damping. Surprisingly, the acceleration time of  $^3\text{He}$  is always shorter than that of  $^4\text{He}$  at nonrelativistic energies. In § 3 the model of SA is briefly summarized and applied to observations of six impulsive solar energetic particle events (SEPs) observed with the *Advanced Composition Explorer (ACE)*, where the low-energy ion spectra have convex shapes, which are referred to as rounded spectra (Mason et al. 2002). Reasonable fits to the observed  $^3\text{He}$  and  $^4\text{He}$  spectra are obtained by adjusting the temperature of the background plasma, the turbulence generation length scale, the intensity of the turbulence, and a normalization factor. In § 3.2 we explore the model parameter space to see how observations can be used to constrain properties of the turbulence and the flaring plasma. It is shown that the acceleration of low-energy  $^4\text{He}$  can still be suppressed, even without the thermal damping effects, because  $^4\text{He}$  interacts mostly with small scale waves that have

relatively low phase velocities. The thermal damping effects just amplify this suppression. The generation length scale of waves in the proton cyclotron (PC) branch determines the acceleration rates at high energies and thus mostly affects the high-energy cutoffs. On the other hand, we show that in more strongly magnetized plasmas the accelerations of  $^4\text{He}$  and  $^3\text{He}$  become comparable, and  $^3\text{He}$  enhancement decreases. This is also true with the increase of the background plasma temperature and/or the intensity of the turbulence. In § 4, we summarize the main results and emphasize the importance of studying the properties of the PC branch in understanding the relative acceleration of  $^3\text{He}$  and  $^4\text{He}$ . The model limitation and future developments of the SA theory are also discussed.

## 2. RESONANT WAVE-PARTICLE INTERACTION

SA of particles by parallel propagating waves has been explored in PL04. For the sake of completeness, we summarize here the main results relevant to current study.

### 2.1. Dispersion Relation and Resonance Condition

To simplify the investigation, we assume that the turbulent plasma waves propagate in a “cold” fully ionized plasma<sup>1</sup>. Then the dispersion relation is determined by the ion abundance and the plasma parameter  $\alpha$ : the ratio of the electron plasma frequency  $\omega_{pe}$  to its gyro-frequency  $\Omega_e$

$$\alpha = \omega_{pe}/\Omega_e = 3.2(n_e/10^{10}\text{cm}^{-3})^{1/2}(B_0/100\text{ G})^{-1}, \quad (1)$$

where  $n_e$  is the electron number density, and  $B_0$  is the large scale magnetic field. In the case of solar flare plasmas, modifications to the dispersion relation due to  $^3\text{He}$  and elements heavier than  $^4\text{He}$  are negligible (Steinacker et al. 1997). For waves propagating parallel to the large scale magnetic fields, one therefore has

$$\frac{k^2}{\omega^2} = 1 - \frac{\alpha^2}{\omega\delta} \left[ \frac{1}{\omega\delta - 1} + \frac{(1 - 2Y_{\text{He}})}{\omega + 1} + \frac{Y_{\text{He}}}{\omega + 1/2} \right], \quad (2)$$

where the fraction of  $^4\text{He}$  number abundance  $Y_{\text{He}} = 0.08$  and  $\delta = m_e/m_p$  is the electron-to-proton mass ratio. The wave frequency and wavenumber are given by  $\omega$  and  $k$  in units

---

<sup>1</sup>As argued in PL04, the inclusion of thermal effects does not change the main conclusions of SA models. These effects in most cases will be overshadowed by the uncertainties in the model parameters describing the spectrum of the turbulence.

of the proton gyro-frequency  $\Omega_p$  and  $\Omega_p/c$ , respectively, where  $c$  is the speed of light. The left-handed polarized waves are designated with a negative frequency, and there are five wave branches (PL04). Figure 1 shows the  $^4\text{He}$ -cyclotron (HeC) and proton-cyclotron (PC) branches, which dominate the SA of  $^3\text{He}$  and  $^4\text{He}$  (LPM04), for three values of  $\alpha$ .

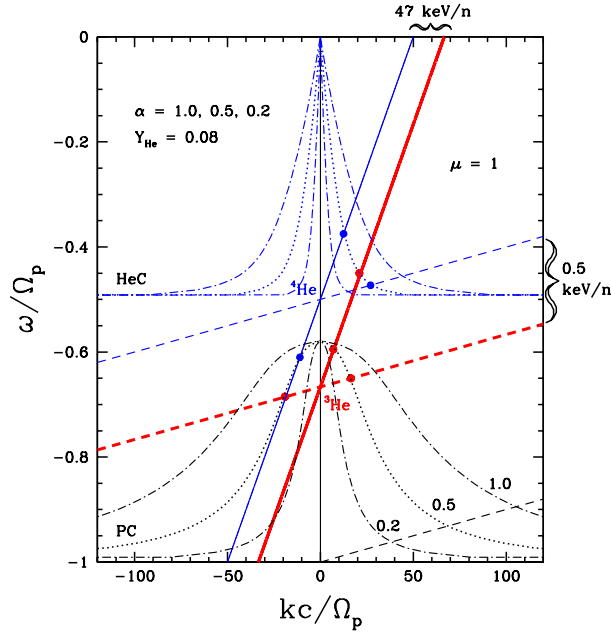


Fig. 1.— Dispersion relations for left-handed polarized parallel propagating waves in the HeC and PC branches for  $Y_{\text{He}} = 0.08$  and for  $\alpha = 1.0$  (*dot-dashed curves*),  $0.5$  (*dotted curves*) and  $0.2$  (*dot-dashed curves*). The solid and dashed lines give the resonance conditions for  $^3\text{He}$  (*thick lower lines*) and  $^4\text{He}$  (*thin upper lines*) with  $\mu = 1.0$  and  $E = 47$  keV/nucleon and  $0.5$  keV/nucleon. The resonant points of these particles with the PC and HeC branches in the plasma with  $\alpha = 0.5$  are designated by the filled circles. The thin dashed line near the bottom indicate the resonance condition for protons with  $\mu = 1.0$  and  $E = 0.5$  keV.

The resonance condition for particles interacting with parallel propagating waves is given by

$$\omega - k\beta\mu = -\frac{\Omega_i}{\Omega_p\gamma}, \quad (3)$$

where  $\beta c$ ,  $\mu$  and  $\gamma$  are the particle velocity, cosine of the pitch angle and Lorentz factor, respectively, and  $\Omega_i$  is the ion gyro-frequency. The straight solid and dashed lines in Figure 1 indicate this relation for  $^3\text{He}$  (*thick lower lines*) and  $^4\text{He}$  (*thin upper lines*) with  $\mu = 1.0$  and two energies. The intersection points of these lines with the dotted lines for the dispersion

relation with  $\alpha = 0.5$  designate waves that satisfy the resonance condition. The Fokker-Planck coefficients for the particles are calculated by adding contributions from these waves (Dung & Petrosian 1994). The dashed line near the bottom gives the resonance condition for 0.5 keV protons with  $\mu = 1$ , which will be useful in understanding the thermal damping effects discussed below.

## 2.2. Turbulence Spectrum

There has been limited work on a complete kinetic theory description of plasma turbulence detailing the wave generation, cascade, and eventually damping by background particles at small scales. Most of the investigations of plasma turbulence are limited to the MHD regime (Bieber et al. 1994; Dröge 2003; Hirose et al. 2004), where the wave frequency is much lower than the particle gyro-frequency, and the turbulence cascade is not isotropic for most of the wave modes (Cho & Lazarian 2003, 2004). A formulation of these processes for application to solar flares is still underdevelopment. Here we study the SA by assuming a power spectrum for the PWT, taking into account the knowledge obtained from recent observations of plasma turbulence in the interplanetary medium and from theoretical investigations. The main features of PWT can be formed by two length scales: the turbulence generation and the wave damping length scale, and the related spectral indexes.

The turbulence generation length scale is usually related to the large scale dynamical evolution of the system, such as the size of the current sheet between reconnecting magnetic fields. For high frequency wave branches, such as the PC branch mentioned above, waves can also be generated via coupling with low frequency MHD waves, like those in the HeC branch (Xie, Ofman, & Viñas 2004). Although the magnetic reconnections and the consequence energy release and turbulence generation processes seem to involve complex micro- and macro- scopic physics, the turbulence generation length size must be smaller than the typical dimension of the system. For flare conditions, such a scale generally implies low wavenumber or frequency waves, which resonate with relativistic particles that is not quite relevant to observations of SEPs with *ACE*. This is the case for the HeC branch so that the low wavenumber cutoff of this branch simply determines the energy content in the turbulence. The PC branch, on the other hand, mostly interacts with nonrelativistic particles. As discussed in PL04 and LPM04, large scale waves in this branch are very efficient accelerators of hundreds of MeV protons,  $^3\text{He}$  and  $^4\text{He}$  ions. Observations of SEPs in this energy range can be used to constrain the wave generation at these length scales. We therefore take the low wavenumber cutoff  $k_{\min}$  of the PC branch as one of the primary model parameters.

The high wavenumber cutoff of the turbulence spectrum is determined by the damping

rate of these waves by the background plasma. Thermal damping involves complicated nonlinear effects (Swanson 1989, pp. 122, 291, and 305), which can change the wave damping rate, modulate the evolution of the wave spectrum at high  $k$ , and the particle distribution in the tail of a thermal background plasma. These determine the injection process of SA. Thermal damping of parallel propagating waves by the background ions has been studied in detail by Steinacker et al. (1997). One of the major findings of this work is that waves that resonate with the high-energy tail of a thermal distribution are subjected to strong Landau damping. Because the abundances of  $^3\text{He}$  and elements heavier than  $^4\text{He}$  are very low, their contributions to the thermal damping effects can be ignored. But for the short scale waves in the HeC and PC branches, which are damped by the background  $^4\text{He}$  and protons, respectively, the decay time could be comparable to the proton gyro-period. A steep turbulence spectrum is expected in this wavenumber range.

We assume that the turbulence is unpolarized and has a broken power-law spectrum for each of five wave branches:

$$\mathcal{E}(k) = (q - 1) \frac{\mathcal{E}_0}{k_{\min}} \begin{cases} (k/k_{\min})^{q_1}, & \text{for } k < k_{\min}, \\ (k/k_{\min})^{-q}, & \text{for } k_{\min} < k < k_{\max}, \\ (k_{\min}/k_{\max})^q (k/k_{\max})^{-q_h}, & \text{for } k > k_{\max}, \end{cases} \quad (4)$$

where  $\mathcal{E}_0$  indicates the intensity of the turbulent plasma waves, and  $k_{\min}$  must be larger (perhaps much larger) than  $k_L \equiv 2\pi c/L\Omega_p$  for a system with size  $L$ . Note that  $\mathcal{E}_0$ ,  $k_{\min}$  and  $k_{\max}$  could be different for different wave branches. However, we assume that the spectral indexes and  $\bar{\mathcal{E}}_0 \equiv (q - 1)\mathcal{E}_0(k_{\min}\delta)^{q-1}$  are the same for all branches so that the wave intensity only depends on the wavenumber  $k$  in the inertial ranges, i.e., between  $k_{\min}$  and  $k_{\max}$ . From the resonance conditions for  $^4\text{He}$  and protons with  $E = 0.5$  keV/nucleon and  $\mu = 1.0$  in Figure 1, we set the high wavenumber cutoff  $k_{\max} = 2\alpha\delta^{-1/2}$  for the PC branch and one half of this value for the HeC branch. This characterizes the damping of waves under plasma conditions typical for solar flares (see Xie et al. 2004). Because the PC branch is the dominant branch here, in what follows the corresponding quantities refer to this branch unless specified otherwise. We choose  $q = 2.0$  and  $q_h = 4.0$  as the fiducial parameters, which are consistent with solar neighborhood observations (Bieber et al. 1994; Dröge 2003)<sup>2</sup>. For  $q = 2.0$  the acceleration and scattering rates of relativistic particles are independent of energy (corresponding to the so-called hard sphere approximation), which gives rise to a power-law particle distribution that is cut off at an energy where the particle resonates with waves with  $k \leq k_{\min}$ , or where a loss process becomes dominant (PL04). Clearly the total turbulence energy density  $\mathcal{E}_{\text{tot}} \simeq 2 \sum_{\sigma} \mathcal{E}_0^{\sigma} = [2\bar{\mathcal{E}}_0/(q - 1)] \sum_{\sigma} (k_{\min}^{\sigma}\delta)^{1-q}$ , where  $\sigma$  indicates the wave

---

<sup>2</sup>The value of  $q_1$  is unimportant as long as it is much larger than 1. We set  $q_1 = 2$  in our calculation.

branches and the factor of 2 arises from the two propagation directions of the waves.

### 2.3. Fokker-Planck Coefficients and Scattering and Acceleration Times

With the turbulence spectrum specified, one can proceed to calculate the Fokker-Planck coefficients (Dung & Petrosian 1994):

$$\left. \begin{array}{l} D_{\mu\mu}^i \\ D_{\mu p}^i \\ D_{pp}^i \end{array} \right\} = \frac{\Omega_i^2 \delta(\mu^{-2} - 1)}{2\Omega_p^2 \gamma^2 \tau_p} \sum_{j=1}^N \chi(k_j) \left\{ \begin{array}{l} \mu\mu(1 - x_j)^2, \\ \mu p x_j(1 - x_j), \\ p^2 x_j^2, \end{array} \right. \quad (5)$$

where

$$\chi(k_j) = \frac{\mathcal{E}(k_j)/\bar{\mathcal{E}}_0}{|\beta\mu - \beta_g(k_j)|}, \quad x_j = \mu\omega_j/\beta k_j, \quad (6)$$

$p$  and  $\Omega_i$  are the particle momentum and gyro-frequency, respectively, and  $\beta_g = d\omega/dk$  is the group velocity of the wave. The sum over  $j$  is for the resonant points discussed above. Following previous studies (Dung & Petrosian 1994; Pryadko & Petrosian 1997; PL04), we describe the turbulence intensity with a characteristic timescale  $\tau_p$

$$\tau_p^{-1} = \pi\Omega_e \left[ \frac{\bar{\mathcal{E}}_0}{B_0^2/8\pi} \right] \quad \text{with} \quad \bar{\mathcal{E}}_0 = \frac{(q-1)\mathcal{E}_{\text{tot}}}{2 \sum_{\sigma} (k_{\text{min}}^{\sigma} \delta)^{1-q}}. \quad (7)$$

Figure 2 gives the dimensionless acceleration rate ( $D_{pp}/p^2$ ) $\tau_p$  (*solid lines*) and scattering rate  $D_{\mu\mu}\tau_p$  (*dashed lines*), as functions of  $\mu$ , for  ${}^3\text{He}$  (*thick lines*) and  ${}^4\text{He}$  (*thin lines*) at  $E = 1$  MeV/nucleon (*left panel*) and 10 keV/nucleon (*right panel*) in a plasma with  $\alpha = 0.5$ . The low wavenumber cutoff of the PC branch  $k_{\text{min}} = 0.1k_{\text{max}} = 0.2\alpha\delta^{-1/2}$  here. The values of the other model parameters introduced above are indicated in the figure. It is obvious that the scattering rate is usually lower than the corresponding acceleration rate. Because of this, to the extent that the acceleration rate depends on  $\mu$ , the particle distribution will be anisotropic, unless there are other scattering agents. More importantly, the acceleration rates of  ${}^3\text{He}$  and  ${}^4\text{He}$  are comparable at 1 MeV/nucleon, but the  ${}^4\text{He}$  acceleration rate is more than 10 times lower than that of  ${}^3\text{He}$  at lower energies, e.g. at 10 keV/nucleon (see the *right panel*). This is because  $D_{pp}$  is proportional to the phase velocity square of the resonant waves and at low energies waves resonating with  ${}^4\text{He}$  have relatively lower phase velocities. Thus, compared with  ${}^3\text{He}$ , the acceleration of  ${}^4\text{He}$  from a low energy can be suppressed significantly.

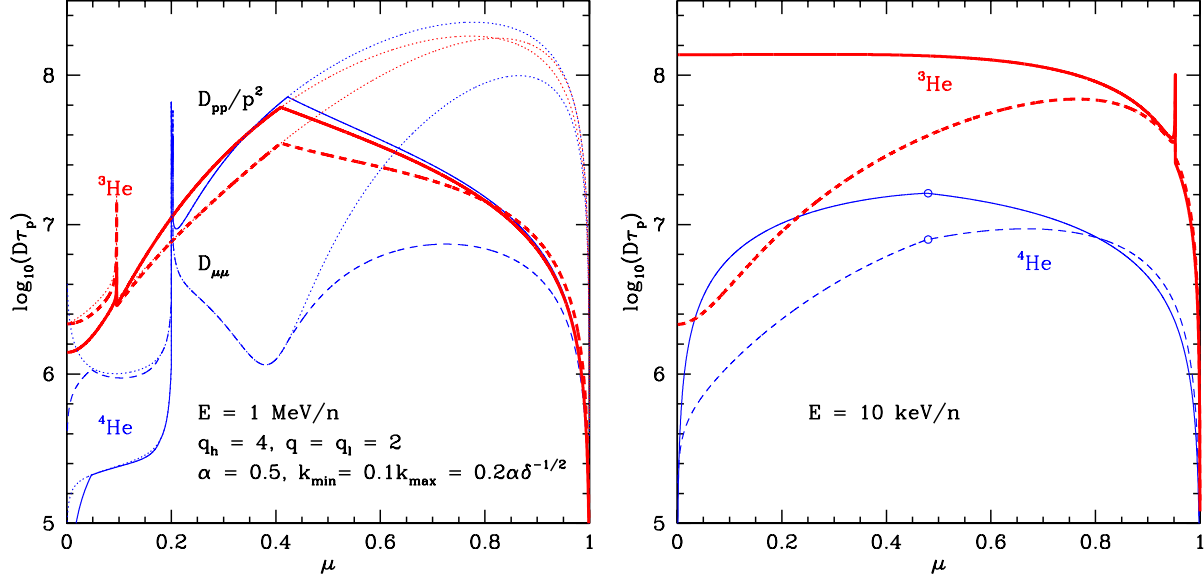


Fig. 2.— *Left*: Pitch angle dependence of the dimensionless scattering ( $D_{\mu\mu}\tau_p$ : *dashed lines*) and acceleration ( $\tau_p D_{pp}/p^2$ : *solid lines*) rates of 1 MeV/nucleon  ${}^3\text{He}$  (*thick lines*) and  ${}^4\text{He}$  (*thin lines*) in a plasma with  $\alpha = 0.5$ . Model parameters are indicated in the figure. The thin dotted lines give the corresponding rates for a pure power-law turbulence spectrum with  $k_{\text{max}} \rightarrow \infty$  and  $k_{\text{min}} \rightarrow k_L$ , or  $q = q_h = 2$  for the model. The small differences at small  $\mu$  from the model with a general broken power-law spectrum are due to the thermal damping effects. The large differences at large  $\mu$  are due to the low wavenumber cutoff  $k_{\text{min}}$ . One sees that the introduction of  $k_{\text{min}} \ll k_L$  can reduce the interaction rates of particles at this energy significantly and the acceleration rate is usually higher than the corresponding scattering rate. *Right*: Same as the left panel, but for  $E = 10$  keV/nucleon particles. The results for a pure power-law turbulence spectrum are not shown. Here the acceleration rate of  ${}^3\text{He}$  is more than one order of magnitude higher than that for  ${}^4\text{He}$ . The open circles indicate breaks caused by  $k_{\text{max}}$ .

To illustrate the effects of introducing the high and low wavenumber cutoffs, the left panel also shows the rates for a pure power-law turbulence spectrum ( $k_{\max} \rightarrow \infty$  and  $k_{\min} \rightarrow k_L$ ), i.e.  $q = q_h = 2$ , as indicated by the thin dotted lines. From the resonance condition (3) one can show that with the thermal damping and reduction of the intensity of high  $k$  waves the interaction rates at small  $\mu$  decreases. The more pronounced differences at large  $\mu$ , on the other hand, are mostly due to the low wavenumber cutoff  $k_{\min}$ . One should also notice that the thermal damping effects reduce the  ${}^4\text{He}$  rates much more than that of  ${}^3\text{He}$ . This can be clearly seen in the right panel, where  $k_{\max}$  introduces a break in the  ${}^4\text{He}$  interaction rates near  $\mu = 0.5$ . No such features are seen in the rates for  ${}^3\text{He}$ . This is expected because  ${}^3\text{He}$  mostly interacts with large scale waves that are not damped. The sharp spikes in the interaction rates are due to the critical angles studied in PL04, when the denominator of equation (6) approaches zero (for interactions with the PC branch). These spikes are very narrow and therefore do not contribute significantly to the pitch angle averaged interaction rates. However, once crossing these spikes, particles start to interact with waves with different phase velocities, and the interaction rate can change dramatically. The left panel illustrates this clearly. At small  $\mu$  the acceleration rate of  ${}^4\text{He}$  is about ten times lower than that of  ${}^3\text{He}$ . Beyond the spike at  $\mu \sim 0.2$  (for  ${}^4\text{He}$ ), the two acceleration rates become comparable since the particles interact with waves with similar frequencies and wavenumbers.

Because the acceleration rate is usually higher than the scattering rate at low energies, one can define the pitch angle averaged acceleration and scattering times (Pryadko & Petrosian 1997):

$$\tau_{\text{ac}} = \frac{2p^2}{\int_{-1}^1 d\mu D_{pp}(\mu)}, \quad (8)$$

$$\tau_{\text{sc}} = \int_{-1}^1 d\mu (1 - \mu^2)^2 / D_{\mu\mu}. \quad (9)$$

Note that here we define  $\tau_{\text{ac}}$  differently from that in LPM04 where we assumed isotropy and that  $D_{\mu\mu} \gg D_{pp}/p^2$ , which is always the case at high energies. But as shown above this is not true at low energies so that the above relation is more accurate. This makes only a quantitative (not a qualitative) difference. Figure 3 shows the energy dependence of these times (acceleration time: *solid lines*, scattering time: *dashed lines*) for  ${}^3\text{He}$  (*thick lines*) and  ${}^4\text{He}$  (*thin lines*) for the model depicted in Figure 2. The scattering time is longer than the corresponding acceleration time below a few MeV/nucleon. First, this implies that at low energies SA is more efficient than diffusive shock acceleration, whose acceleration time is comparable to the scattering time. We also expect some anisotropy in accelerated particle distributions with a pitch angle distribution similar to the pitch angle dependence of the acceleration rates. However, as shown in Figure 2 the expected anisotropy will not

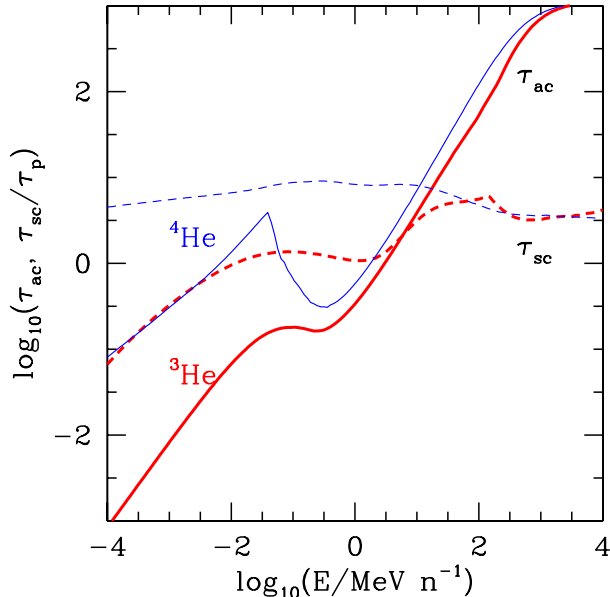


Fig. 3.— The energy dependence of pitch angle averaged scattering (*dashed lines*) and acceleration (*solid lines*) times for  $^4\text{He}$  (*thin lines*) and  $^3\text{He}$  (*thick lines*). The model parameters are the same as those in Figure 2.

be large, and other scattering processes, such as Coulomb collisions, may further isotropize the accelerated particle distribution. Beyond a few tens of MeV/nucleon scattering becomes more efficient, and isotropy of the particle distribution is established by wave scatterings.

Below a few tens of keV/nucleon the acceleration time of  $^4\text{He}$  is more than one order of magnitude longer than that of  $^3\text{He}$ . The sharp decrease of the  $^4\text{He}$  acceleration time near 40 keV/nucleon is due to the interaction of  $^4\text{He}$  with large scale waves in the PC branch, which also dominate the acceleration of  $^3\text{He}$  (see Fig. 1). The acceleration times of the two particles become comparable beyond 100 keV/nucleon and are identical at relativistic energies.

#### 2.4. Dependence of Acceleration Times on Model Parameters

The physical conditions for different solar flares are expected to be different. In this section we investigate how the acceleration times depend on the model parameters.

As discussed above, we parameterize the wave spectrum by several parameters with

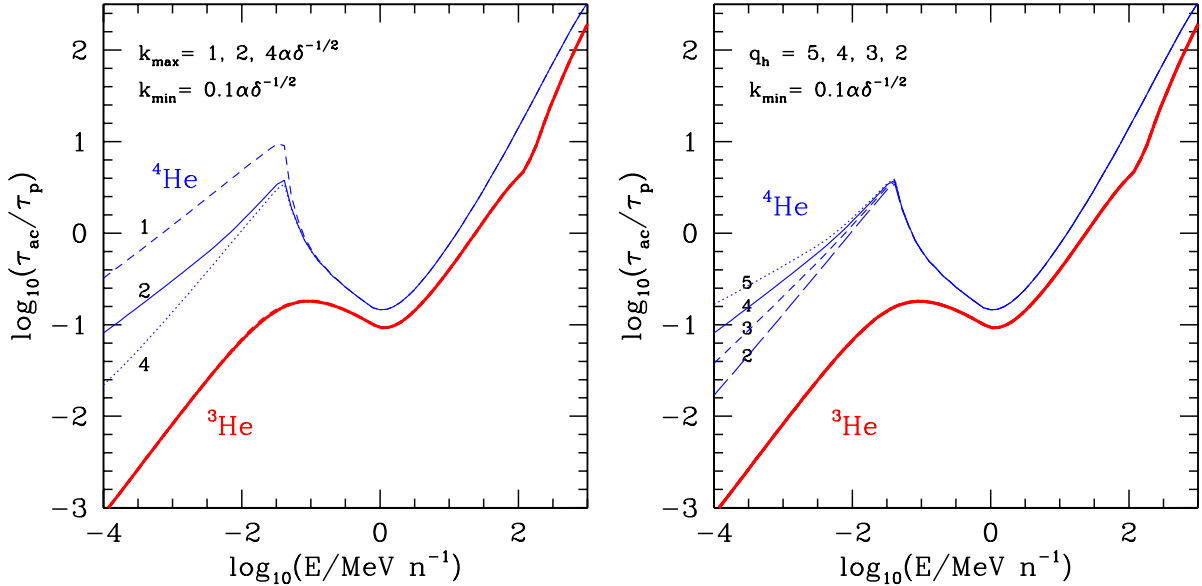


Fig. 4.— *Left*: Dependence of the acceleration time of  ${}^4\text{He}$  on the high wavenumber cutoff  $k_{\max}$  with  $k_{\min} = 0.1\alpha\delta^{-1/2}$ . Note that acceleration of  ${}^3\text{He}$  is not affected. Other model parameters are the same as those in Figure 2. The solid lines are similar to those in Figure 3 except for the difference due to a lower  $k_{\min}$  adopted here. In what follows we choose this as the fiducial model (always indicated by solid lines). The high wavenumber cutoff for the PC branch is always two times higher than that for the HeC branch. The lines are labeled with their corresponding  $k_{\max}$  in units of  $\alpha\delta^{-1/2}$ . The dashed line is for  $k_{\max} = \alpha\delta^{-1/2}$  and the dotted lines for a four times higher  $k_{\max}$ . *Right*: Same as the left panel except that here the dependence on the spectral index  $q_h$  is shown. Note that the  $q_h = 2$  model has no thermal damping.

two of them characterizing the thermal damping; namely the high wavenumber cutoff  $k_{\max}$  and the turbulence spectral index  $q_h$ . Figure 4 shows how the acceleration times of  ${}^3\text{He}$  and  ${}^4\text{He}$  change with these parameters. The left panel is for different  $k_{\max}$ , and the right panel has different  $q_h$ . Here the solid lines represent our fiducial model, which is analogous to that in Figure 3 except that the low wavenumber cutoff  $k_{\min}$  is now two times lower:  $k_{\min} = 0.1\alpha\delta^{-1/2}$ .

One obvious feature is that the thermal damping does not affect the acceleration time of  ${}^3\text{He}$ . As mentioned above, this is because  ${}^3\text{He}$  mostly interacts with large scale waves in the PC branch, which can not be damped by the low-energy protons and  $\alpha$ -particles in the

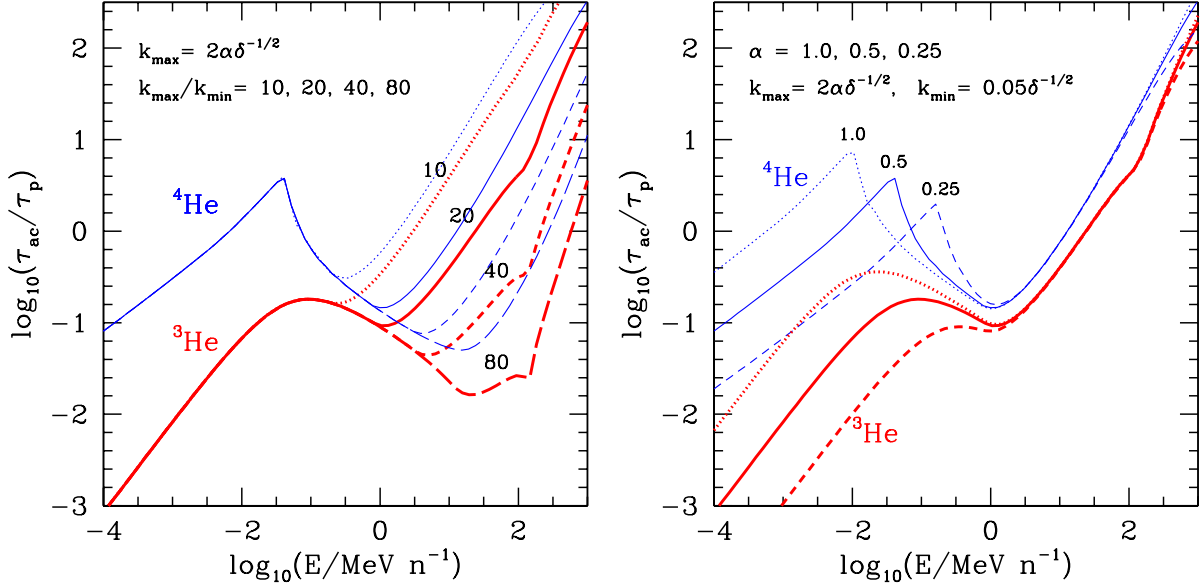


Fig. 5.— Same as Fig. 4 but showing the dependence of the acceleration times on  $k_{\min}$  (left) and the plasma parameter  $\alpha$  (right). Here  $k_{\max}$  changes with  $\alpha$  (See Fig. 1), but all other model parameters remain the same as in the fiducial model.

background. The lower  $k_{\max}$  and the larger  $q_h$ , the stronger the thermal damping, and, as expected, the longer the acceleration time of  ${}^4\text{He}$ . Higher energy particle acceleration time is not affected by the damping because these particles interact with low wavenumber waves. We also note that the acceleration time of  ${}^4\text{He}$  at low energies is more sensitive to  $k_{\max}$  than to  $q_h$ . Even in the case  $q_h = 2$ , which corresponds to the absence of damping effects, the  ${}^4\text{He}$  acceleration time is still more than ten times longer than the  ${}^3\text{He}$  acceleration time at low energies. So the  ${}^4\text{He}$  acceleration from a low energy can be suppressed even without the thermal damping effects. This suppression is purely because of the modification to the dispersion by the presence in the plasma of a significant population of  $\alpha$ -particles, and only depends on the plasma parameter  $\alpha$  and the  ${}^4\text{He}$  abundance  $Y_{\text{He}}$ .

As mentioned earlier, the generation length of waves in the PC branch, corresponding to  $k_{\min}$ , is another important parameter. The left panel of Figure 5 shows how  $k_{\min}$  affects the acceleration times. (The low wavenumber cutoffs of other branches are assumed to be far lower so that they do not affect the acceleration of nonrelativistic particles.) Obviously these large scale waves mostly interact with particles in the MeV/nucleon energy range, so that the acceleration times at low energies remain unchanged. However the acceleration

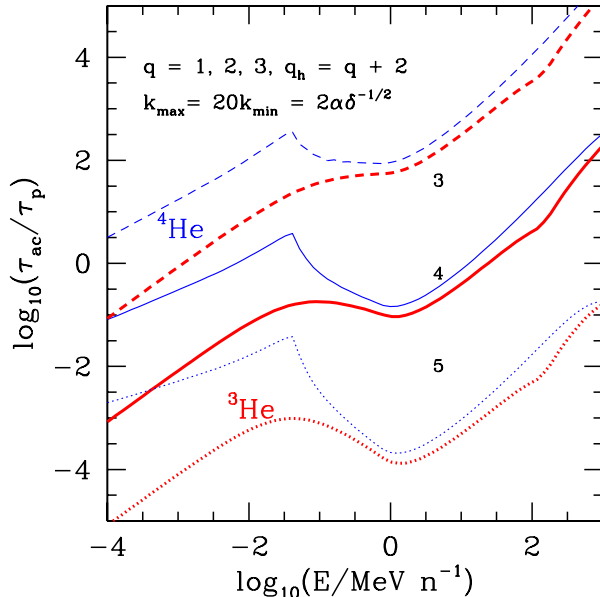


Fig. 6.— Same as Fig. 4 except for the dependence of the acceleration times on the turbulence spectral indexes  $q$  and  $q_h$ .  $q_h - q = 2$ . All other model parameters remain the same as the fiducial model.

of MeV/nucleon particles is very sensitive to this parameter for both  $^3\text{He}$  and  $^4\text{He}$ . With the decrease of  $k_{\min}$  particle acceleration at high energies becomes more efficient but the relative rate of the two ions changes very little. In the following sections we show that the high-energy cutoffs of the accelerated particle spectra are very sensitive to this parameter and observations with *ACE* can be used to constrain it directly.

The right panel of Figure 5 shows the dependence of the acceleration time on the plasma parameter  $\alpha$ . The most prominent feature of these curves is the decrease of  $\tau_{\text{ac}}$  for both ions at low energies with the decrease of  $\alpha$ . This does not affect the  $^3\text{He}$  acceleration but has important effects on the  $^4\text{He}$  acceleration because of its long  $\tau_{\text{ac}}$  (see § 3.2). Because  $k_{\min}$  is fixed, the acceleration times in the MeV/nucleon energy range do not change significantly. The plasma parameter, therefore, mostly affects the acceleration rates at low energies and the relative acceleration of the ions.

Figure 6 shows how the acceleration times change with the turbulence spectral indexes  $q$ . Here we keep  $q_h - q = 2$  and other model parameters unchanged in these calculations. As expected, the acceleration of high-energy particles becomes more efficient when the turbulence spectrum becomes steeper since high-energy particles mostly resonate with large scale

waves (eq. [3]). (Note that the normalization time  $\tau_p$  changes with  $q$ .) Surprisingly, however, for all the model parameters considered here the acceleration time of  $^4\text{He}$  is always longer than the  $^3\text{He}$  acceleration time. This is one of the key features of SA by parallel propagating waves and has profound implications on the enhancement of  $^3\text{He}$  and the relative acceleration of the two species.

### 3. MODEL DESCRIPTION AND APPLICATION TO SEPS

In the SA theory ions gain energy via their resonant interactions with the PWT and lose energy via Coulomb collisions with the background thermal particles. These processes can be described by the Fokker-Planck equation, whose coefficients have been calculated in the previous section for interactions with parallel propagating waves under the quasi-linear approximation and where the perpendicular diffusion across magnetic field lines is ignored. When the wave-ion scattering rate is comparable to the ion acceleration rate, in principle one needs to solve the four-dimensional equation for the particle phase space distribution with the time  $t$ , momentum  $p$ , pitch angle cosine  $\mu$ , and the location along the large scale magnetic field line  $s$  as variables. But the problem can be simplified considerably when one of the rates is much higher than the other (Pryadko & Petrosian 1997). This is the case in the low- and high- energy limits considered here, where the acceleration rate and scattering rate dominate, respectively. Moreover, if the pitch angle dependence of the diffusion coefficients is weak (e.g. peaked in a narrow range of  $\mu$ , see Fig. 2), then the pitch angle distribution of the particles will be relatively smooth and the anisotropy will be small so that one can use pitch angle averaged quantities. Furthermore, because we are mostly interested in the spatially integrated spectra, we can also integrate the particle distribution spatially (along the field lines). Then the acceleration of particles from a low-energy thermal background to relativistic energies can be treated fairly accurately by the well-known equation

$$\frac{\partial N}{\partial t} = \frac{\partial^2}{\partial \varepsilon^2} (D_{\varepsilon\varepsilon} N) + \frac{\partial}{\partial \varepsilon} [(\dot{\varepsilon}_L - A(\varepsilon))N] - \frac{N}{T_{\text{esc}}} + \dot{Q}, \quad (10)$$

where  $N(\varepsilon)$  is the pitch angle averaged and spatially integrated distribution of accelerated particles with kinetic energy  $\varepsilon$ ,  $D_{\varepsilon\varepsilon} = \varepsilon^2 \tau_{\text{ac}}^{-1}$  is the pitch angle and spatially averaged diffusion rate, and  $A(\varepsilon) = dD_{\varepsilon\varepsilon}/d\varepsilon + D_{\varepsilon\varepsilon}(2 - \gamma^{-2})/\varepsilon(1 + \gamma^{-1})$  is the direct acceleration rate. The loss rate  $\dot{\varepsilon}_L$  due to Coulomb collisions is summarized in PL04. The escape time  $T_{\text{esc}} = L/2^{1/2}v + L^2/v^2\tau_{\text{sc}}$  describes the spatial diffusion of the particles along the large scale magnetic field lines.  $\dot{Q}$  is a spatially integrated source term, which we identify as the thermal background plasma. For quantitative modeling, one needs to specify the length of the acceleration region  $L$  and the background plasma density  $n_e$ , magnetic field  $B_0$ , and temperature  $T$ , which we assume is the same for all background charged particles.

Each term in equation (10) can be characterized by an energy dependent timescale. The timescale of source particle injection  $\dot{Q}$  is determined by the large scale dynamical evolution of the system, which is comparable to the modulation timescale of the solar flare. Because the other interaction times are usually much shorter than the dynamical time of the system, one only needs to consider the steady-state solution of the equation with  $\dot{Q} = \text{constant}$ . Then the escaping flux  $f = N/T_{\text{esc}}$  can be compared with the observed fluences of SEPs with a normalization factor taking into account the duration of the flare and the cross sectional area of the flaring magnetic fields. (Note that for the impulsive SEPs studied here, the transport effects of the ions from the flaring site in the solar corona to *ACE* in the earth’s neighborhood are negligible because their scattering mean free path is long [Mason et al. 1989, 2002].) To appreciate spectral features of the corresponding solutions, besides the escape time mentioned above, we also define a loss time  $\tau_{\text{loss}} = \varepsilon/\dot{\varepsilon}_L$  and a direct acceleration time  $\tau_a = \varepsilon/A \sim \tau_{\text{ac}}$  for the second term on the right-hand side of equation (10). Then the ion loss time as a function of the ion kinetic energy per nucleon is proportional to the ion atomic number and is inversely proportional to the square of the ion charge (PL04).

### 3.1. Spectral Fit

The left panel of Figure 7 shows these timescales for a model with  $L = 2 \times 10^9$  cm,  $B_0 = 200$  G,  $n_e = 9 \times 10^8$  cm<sup>-3</sup>, the temperature of the background plasma  $k_B T = 0.26$  keV, and the characteristic timescale  $\tau_p^{-1} = 5.5 \times 10^{-3}$  s<sup>-1</sup>. All other model parameters are the same as in Figure 3. The corresponding plasma parameter  $\alpha = 0.48$ , and  $8\pi\bar{\mathcal{E}}_0/B_0^2 = 4.9 \times 10^{-13}$ . The total turbulence energy density can be very low if the generation length scale of waves in the HeC branch is much shorter than  $L$ . All these parameters are typical for solar flares, and a weak level of turbulence also justifies the quasi-linear approximation adopted here and is consistent with the general view that the flares are powered by energies stored in the pre-flare magnetic fields presumably via magnetic reconnections. The right panel shows the model fit to the observed <sup>3</sup>He and <sup>4</sup>He spectra of an impulsive SEP on 1999 September 30 observed with *ACE*. The injected (background) plasma is assumed to have a solar abundance so that the number of <sup>3</sup>He ions integrated over the whole energy range is 2000 times fewer than that of <sup>4</sup>He. The model clearly produces the observed extreme enhancement of <sup>3</sup>He and gives a reasonable fit to the spectra of both ions.

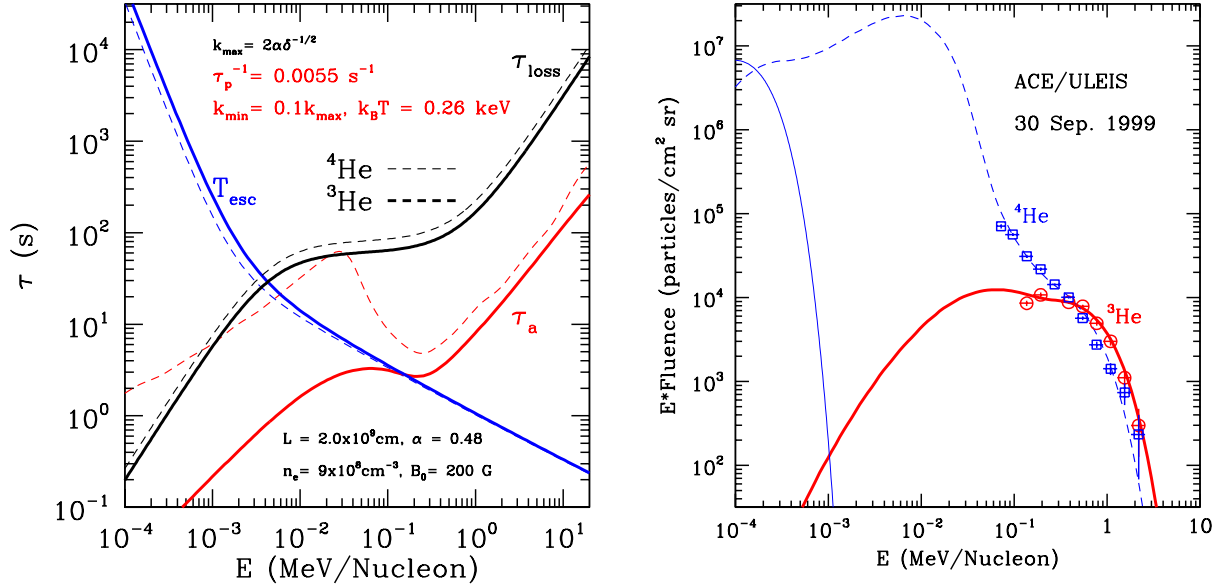


Fig. 7.— *Left*: Direct acceleration ( $\tau_a$ ), loss ( $\tau_{\text{loss}}$ ), and escape ( $T_{\text{esc}}$ ) times, as functions of the particle kinetic energy per nucleon, for  ${}^3\text{He}$  (*solid lines*) and  ${}^4\text{He}$  (*dashed lines*) ions in a SA model for the event on 1999 September 30. Model parameters are indicated in the figure. The acceleration times are very similar to those of the model in Figure 3. The loss term is dominated by Coulomb collisions with background protons below  $\sim 10$  keV/nucleon and with electrons above it. The loss time in the tens of keV/nucleon energy range is very sensitive to the temperature of the background electrons ( $\propto T^{3/2}$ ). The sharp increase of the escape times with the decrease of energy below a few keV/nucleon is due to the suppression of the particle spatial diffusion rate by efficient Coulomb scatterings, whose rate is comparable to the ion energy loss rate. Scatterings are unimportant at high energies so that  $T_{\text{esc}} \simeq L/2^{1/2}v$ . *Right*: The corresponding model fit to the observed  ${}^3\text{He}$  (*circles*) and  ${}^4\text{He}$  (*squares*) spectra. The thin solid line gives the distribution of the injected thermal  $\alpha$ -particles with arbitrary normalization. (Note that the temperatures of both background ions are equal.)

Because the acceleration time of  ${}^3\text{He}$  is always much shorter than its Coulomb loss time, the accelerated spectrum is determined by the acceleration and escape terms. Injected at a very low energy, almost all thermal ( $k_{\text{B}}T = 0.26$  keV)  ${}^3\text{He}$  particles are accelerated to the hundreds of keV/nucleon energy range, where the escape process starts to dominate over the acceleration process. The sharp spectral cutoff near 1 MeV/nucleon results from the quick divergence of the acceleration and the escape times above this energy. The SA acceleration is effectively quenched at higher energies. The acceleration of  ${}^4\text{He}$ , on the other hand, is quite different. The acceleration time of  ${}^4\text{He}$  is comparable with its loss time below a few tens of keV/nucleon. Near the energy of the injected thermal particles,  $A(\varepsilon) \leq \dot{\varepsilon}_{\text{L}}$  and the direct acceleration is difficult, the energy diffusion term on the right-hand side of equation (10) dominates the acceleration processes so that more than half of the injected particles are accelerated to energies  $> 1$  keV/nucleon. However, the escape time becomes much shorter than the other times between 10 and 100 keV/nucleon, resulting in a very steep spectrum beyond  $\sim 10$  keV/nucleon. Consequently most of the accelerated  $\alpha$ -particles stay below  $\sim 10$  keV/nucleon. This suppresses the acceleration of  ${}^4\text{He}$  ions to higher energies and gives rise to the observed enhancement of  ${}^3\text{He}$  ions in the MeV/nucleon energy range. At a few hundreds of keV/nucleon the  ${}^4\text{He}$  acceleration time becomes comparable with its escape time due to very efficient acceleration by large scale waves in the PC branch. This gives rise to a relative hard accelerated  ${}^4\text{He}$  spectrum. However, because the  ${}^4\text{He}$  acceleration time is always longer than that of  ${}^3\text{He}$ , its spectrum is always softer than the spectrum of accelerated  ${}^3\text{He}$  ions.

The achievements of the model in explaining the 1999 September 30 event tempt us to apply it to other impulsive SEPs. We first consider the events with the so-called rounded spectra, as suggested by the model calculations above (Fig. 7). Another five such impulsive events are found during the *ACE* observation period from 1998 to 2000. These events show quite different  ${}^3\text{He}$  enhancement, and the location of the high-energy cutoffs of the spectra varies considerably (Figure 8).

In the previous section we have shown that the relative acceleration of  ${}^3\text{He}$  and  ${}^4\text{He}$  is controlled by the thermal damping of waves at small scales since these damping effects only modify the acceleration rate of  ${}^4\text{He}$  at low energies. In the application of the SA model to the event studied above, we find that the acceleration of  ${}^3\text{He}$  is quite insensitive to the temperature of the injected plasma because its acceleration time is always much shorter than its loss time. However, the acceleration of  ${}^4\text{He}$  can be suppressed dramatically as  $T$  decreases because of the difficulty in the direct acceleration at low energies. The three model parameters,  $T$ ,  $k_{\text{max}}$ , and  $q_{\text{h}}$ , thus have the equivalent function of controlling the acceleration of low-energy  ${}^4\text{He}$ , and consequently the enhancement of  ${}^3\text{He}$ . These three parameters are all related to the thermal damping processes of plasma waves. For a given energy input rate into the turbulence at large scales, the value of  $k_{\text{max}}$  and  $q_{\text{h}}$  should only depend on  $T$ . In

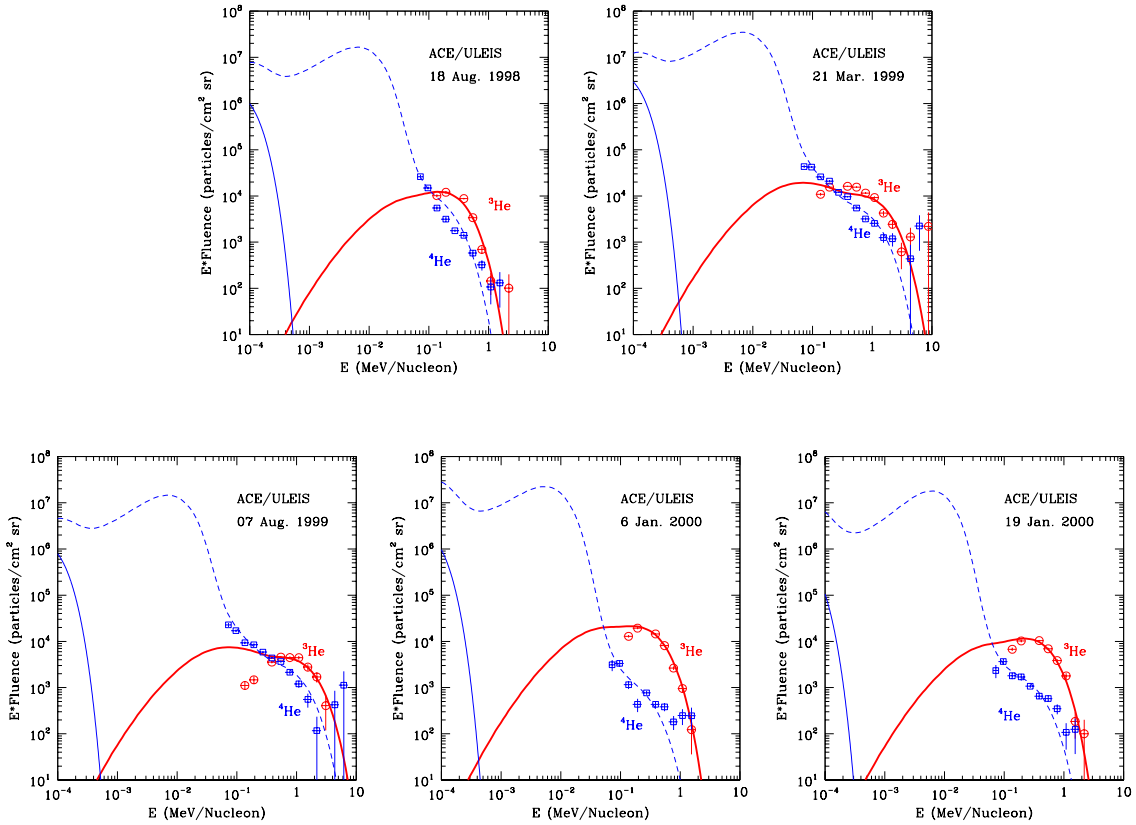


Fig. 8.— Same as the right panel of Figure 7, but for five impulsive SEP events with convex  ${}^3\text{He}$  spectra observed by *ACE* between 1998 and 2000. The model parameters are listed in Table 1. See text for details.

what follows we assume that  $k_{\text{max}}$  and  $q_{\text{h}}$  weakly depend on the turbulence energy density and  $T$  and fix them to the values used for the event shown in Figure 7. The corresponding effective temperature of the injected plasma  $T_{\text{eff}}$  is used to adjust the enhancement of  ${}^3\text{He}$  (or more accurately the suppression of accelerated  ${}^4\text{He}$ ).

The analyses of the wave-particle interactions in the previous section also suggest that the high-energy cutoff of the accelerated ion spectra is likely related to the generation length of waves in the PC branch. We therefore leave  $k_{\text{min}}$  as another primary model parameter to account for the observed variations of the ion high-energy spectral cutoffs. For different solar flares  $\tau_p$  and other model parameters will also change. We adjust  $\tau_p$  and the normalization factor for the total amount of the injected particles  $N_0 \propto \dot{Q}$  to finalize the spectral fitting, but in order to reduce the amount of calculation we keep all other model parameters the

same as those in the above model. Figure 8 shows the model fit to the spectra of these five events. The corresponding model parameters are list in table 1. The models in general give reasonable spectral fits to the five events, and reproduce their varied degree of  $^3\text{He}$  enhancement. There are, however, obvious discrepancies in the low-energy  $^3\text{He}$  spectrum of the 1999 August 7 event and the high-energy  $^4\text{He}$  spectra of the 2000 events.

Table 1: Events and the Corresponding Model Parameters.

Events	$k_{\min}/k_{\max}$	$\tau_p^{-1}/10^{-3}\text{s}^{-1}$	$k_{\text{B}}T_{\text{eff}}/\text{keV}$	$N_0^\dagger$
1998 Aug 18	0.16	6.0	0.12	0.79
1999 Mar 21	0.075	6.0	0.14	1.6
1999 Aug 7	0.075	6.5	0.12	0.63
1999 Sep 30	0.10	5.5	0.26	1
2000 Jan 6	0.14	5.5	0.10	1.6
2000 Jan 19	0.14	7.5	0.07	0.79

---

<sup>†</sup>The normalization is with respect to the event on 1999 September 30.

Note. — The other model parameters are the same as those for the 1999 September 30 event, i.e.  $L = 2 \times 10^9$  cm,  $B_0 = 200$  G,  $n_e = 9 \times 10^8$  cm $^{-3}$  (therefore  $\alpha = 0.48$ ),  $k_{\max} = 2\alpha\delta^{-1/2}c\Omega_p^{-1}$  for the PC branch and one half of it for the HeC branch,  $q_l = 2$ ,  $q = 2$ , and  $q_h = 4$ .

For the six events studied here the effective temperature of the injected plasma varies within a factor of 4. Because the  $^3\text{He}$  enhancement decreases with the increase of  $T_{\text{eff}}$  (see discussions above and more quantitative studies in the next section), and the thermal damping effects are enhanced with temperature, we expect more significant variations in the real temperatures of the background plasmas for these events except that there is a positive correlation between the temperature  $T$  and the turbulence energy density (indicated by the value of  $\tau_p^{-1}$ , which is anti-correlated with the  $^3\text{He}$  enhancement, because  $^3\text{He}$  can be accelerated to high energies even with large  $\tau_p$  while  $^4\text{He}$  can not). The “generation” length scale or  $k_{\min}$  of the waves in the PC branch changes within a factor of 2.2, which seems to be a reasonable range. The characteristic timescale  $\tau_p$  has much less variations (about 30%), which may be due to the similarities of the rounded spectra of these events and the comparable amplitude of the events as indicated by the relative normalization factor in the last column, which varies within a factor of 3.

### 3.2. Exploring of Model Parameters Space

In the previous section we have shown that the observed degree of enhancement and the primary features of the rounded spectra of  $^3\text{He}$  and  $^4\text{He}$  can be reproduced in our model with reasonable values of the parameters. Here we describe the dependence of these observed characteristics on various parameters.

#### 3.2.1. Turbulence Spectrum and Thermal Damping

One of the most uncertain part of the model is related to the characteristics of turbulence. The two model parameters  $k_{\text{max}}$  and  $q_{\text{h}}$  characterize the wave damping process. The background temperature which plays important roles in this damping process also has important influence. As mentioned above, thermal damping that involves complicated nonlinear processes determines the connections among these parameters (Yan, Petrosian, & Lazarian 2005). Investigation of these aspects is beyond the scope of this paper. Here we consider the influence of these parameters separately. In Figure 9 we show the effects of the above mentioned parameters, while keeping other parameters constant and equal to those in Figure 7. The enhancement of  $^3\text{He}$  (or equivalently the suppression of  $^4\text{He}$  acceleration) decreases rapidly with increasing  $T$  at low values of  $T$ , primarily because the number of  $^4\text{He}$  in the energy range where  $\tau_{\text{loss}} < \tau_{\text{a}}$  decreases exponentially with  $T$ . However, even with a high temperature, the acceleration of  $^4\text{He}$  is still suppressed because its escape process dominates in the tens of keV energy range, and the  $^3\text{He}$  enhancement eventually saturates. The saturation level depends on the other parameters. For higher values of  $k_{\text{max}}$  and lower  $q_{\text{h}}$  (indicating slower damping) the enhancement of  $^3\text{He}$  is smaller. But for the range of values explored here, there is always a significant enhancement. Even in the case without thermal damping effects, i.e. for  $q_{\text{h}} = 2$ , strong  $^3\text{He}$  enhancement can still be produced, which underscores the importance of using the exact dispersion relation in modeling the wave-particle interactions (LPM04). The thermal damping affects primarily the  $^3\text{He}$  to  $^4\text{He}$  ratio, but introduces minor changes in the spectrum of accelerated ions (specially  $^3\text{He}$ ) (*middle and right* panels).

The dot-dashed horizontal line in Figure 9 indicates the observed range of  $^3\text{He}$  enhancement. The spectral indexes vary from -1 to -4. The lack of observations with even higher  $^3\text{He}$  to  $^4\text{He}$  ratio speaks against models with small  $k_{\text{max}}$  (or very strong damping) and low temperatures of the background plasmas. More detailed theoretical investigations of the wave damping should be able to resolve this issue and give better constraints on the SA model.

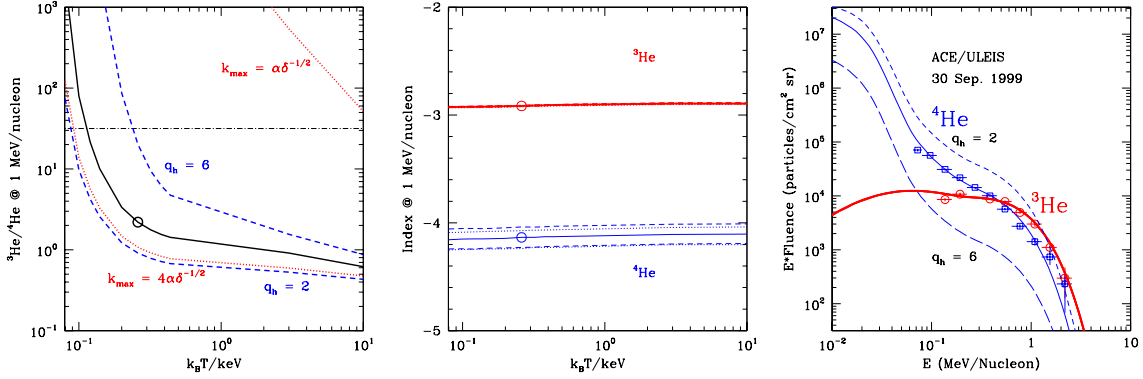


Fig. 9.— *Left*: Dependence of the  ${}^3\text{He}$  to  ${}^4\text{He}$  ratio at 1 MeV/nucleon on the temperature of the injected plasma for several models with different turbulence spectra. The solid line corresponds to the fiducial model for the 1999 September 30 event, which is indicated by the large open circle. The dotted lines are for two models with  $k_{\text{max}} = \alpha\delta^{-1/2}$  (*upper one*) and  $4\alpha\delta^{-1/2}$  (*lower one*). The other model parameters are the same as those for the solid line. The same is true for the dashed lines except now  $q_h = 6$  (*upper one*) and 2 (*lower one*). The latter has no thermal damping. The horizontal dot-dashed line gives the highest  ${}^3\text{He}$  enhancement observed so far, corresponding to the event on 2000 January 6. Most of the models with strong damping ( $k_{\text{max}} = \alpha\delta^{-1/2}$ ) or very low temperatures ( $< 10^6$  K) can be ruled out because the very high predicted  ${}^3\text{He}$  enhancement has never been observed. *Middle*: Same as the left panel except for the spectral indexes of  ${}^3\text{He}$  (*thick lines*) and  ${}^4\text{He}$  (*thin lines*) defined as  $d \ln f / d \ln E$  at 1 MeV/nucleon. *Right*: The dependence of the accelerated  ${}^3\text{He}$  and  ${}^4\text{He}$  spectra on  $q_h$ . The upper dotted line is for  ${}^4\text{He}$  and  $q_h = 2$  and corresponds to the case without thermal damping. The lower dotted line is for  $q_h = 6$ . The solid and dashed lines and the data points correspond to the fiducial model shown in the right panel of Figure 7. All other model parameters remain the same. The  ${}^3\text{He}$  acceleration is not affected by  $q_h$ .

### 3.2.2. Turbulence Strength and Scale

The “generation” length scale of waves in the PC branch, characterized by  $k_{\min}$ , and the turbulence intensity, proportional to  $\tau_p^{-1}$ , are two other important parameters characterizing the PWT. Figure 10 shows the dependence of the  ${}^3\text{He}$  enhancement and the accelerated spectra of  ${}^3\text{He}$  and  ${}^4\text{He}$  on these parameters. In general, again almost all of the injected  ${}^3\text{He}$  ions are accelerated to high energies, but the acceleration of low-energy  ${}^4\text{He}$  ions is very sensitive to  $\tau_p^{-1}$  specially at low  $\tau_p^{-1}$ . Therefore, the  ${}^3\text{He}$  to  ${}^4\text{He}$  ratio at high energies decreases rapidly with the increase of the turbulence intensity. With very strong turbulence ( $\tau_p^{-1} \geq 0.1$ ), almost all of the injected  $\alpha$ -particles could be accelerated to high energies, and there is essentially no  ${}^3\text{He}$  enhancement (see *left panel*). The high-energy spectra of the accelerated particles are also very sensitive to  $\tau_p^{-1}$  and  $k_{\min}$ . With the increase of  $\tau_p^{-1}$ , the spectra become harder (*middle panel*). But for low values of  $k_{\min}$ , the cutoff energies of the accelerated ions will increase with minimal effects on the shapes of the spectra at lower energies (*right panel*).

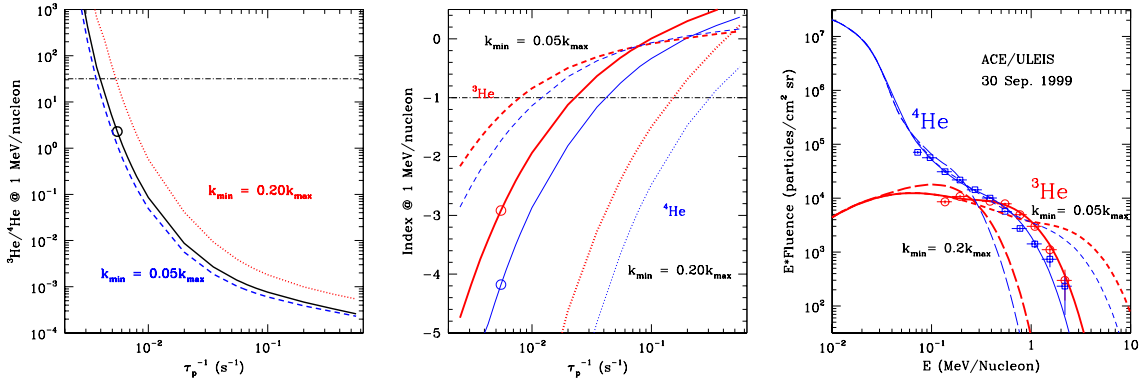


Fig. 10.— Same as Figure 9. *Left*: for the dependence on  $\tau_p^{-1}$  and for two dynamic ranges  $k_{\min}/k_{\max} = 0.2$  (*upper dotted line*) and  $0.05$  (*lower dashed line*) with a fixed  $k_{\max} = 2\alpha\delta^{-1/2}$ . Events with weak turbulence have high  ${}^3\text{He}$  enhancement and soft spectra. With very strong turbulence ( $\tau_p^{-1} \geq 0.1$ ), all of the injected  ${}^3\text{He}$  and  ${}^4\text{He}$  are accelerated to high energies, and  ${}^3\text{He}$  enhancement disappears. *Middle*: Here the dashed lines are for  $k_{\min} = 0.1\alpha\delta^{-1/2}$  and the dotted lines are for  $k_{\min} = 0.4\alpha\delta^{-1/2}$ . *Right*: The dependence of spectra on  $k_{\min}$  showing that for lower  $k_{\min}$  the spectra cut off at higher energies. The thinner lines are for  ${}^4\text{He}$  and the thicker for  ${}^3\text{He}$ .

### 3.2.3. Background Plasma Parameters

Besides the temperature, other characteristics of the background plasma also affect the particle acceleration, with the main parameter being the plasma parameter  $\alpha$ . To change  $\alpha$  we keep the density, which affects the loss and escape processes at low energies, constant and change the large scale magnetic field  $B_0$ . Figure 11 depicts the influence of  $\alpha$ . Following the right panel of Figure 5, we keep  $k_{\max}/\alpha$  and all other model parameters unchanged. As expected,  $\alpha$  predominately affects the ion acceleration in the low-energy range. The  ${}^3\text{He}$  enhancement decreases with the decrease of  $\alpha$ , corresponding to more strongly magnetized plasmas. The  $\tau_p$  dependence of the  ${}^3\text{He}$  to  ${}^4\text{He}$  ratio at 1 MeV/nucleon is quite different for different values of  $\alpha$ , especially when  $\tau_p^{-1}$  is small (*left panel*). The high-energy spectral indexes, however, are only weakly dependent on  $\alpha$  (*middle panel*). The right panel shows explicitly that the acceleration of low-energy ions, specially  ${}^4\text{He}$ , becomes more efficient in more strongly magnetized plasmas.

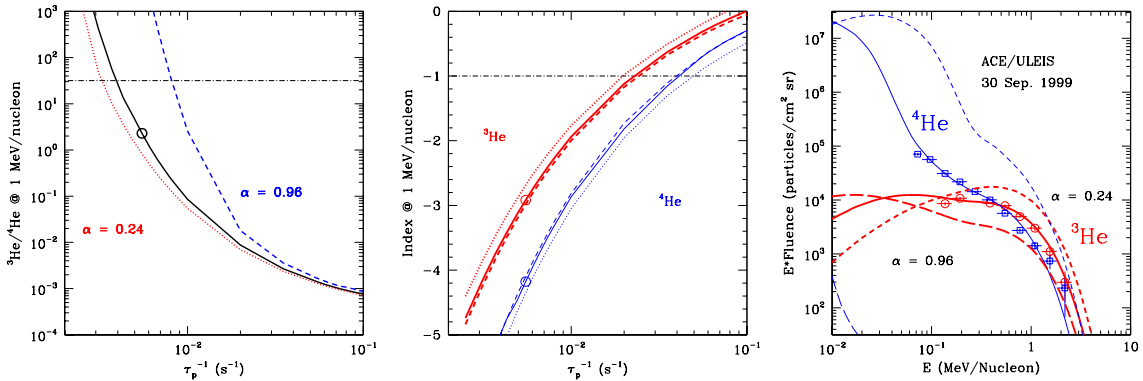


Fig. 11.— Same as Figure 10, but for models with different plasma parameter  $\alpha$ . Here the dashed and dotted lines in the left and middle panels are for  $\alpha = 0.96$  and  $0.24$ , respectively. Different values of  $\alpha$  are achieved by adjusting the large scale magnetic field  $B_0$ , which affects the particle acceleration only via  $\alpha$ . The gas density  $n$  remains the same so that the loss and escape times do not change. All other model parameters and  $k_{\max}/\alpha$  also remain the same. Models with larger  $\alpha$  have less efficient particle acceleration at low energies, giving rise to softer low-energy spectra (*right*). (Note that because the  ${}^4\text{He}$  acceleration is very inefficient in the case of  $\alpha = 0.96$ , the spectrum of the accelerated  $\alpha$ -particle is barely seen at the low left corner in the figure.) The high-energy spectral shape is not very sensitive to  $\alpha$  (*middle*).

#### 4. SUMMARY AND CONCLUSION

Recent observations of SEPs and radiations produced by solar flares indicate that SA may play a major important role in the acceleration of all particles. It has been applied extensively to impulsive SEPs, and may be involved in the pre-acceleration of particles in gradual flares, where the particles are further accelerated to even higher energies by interplanetary shocks (Desai et al. 2001, 2003, 2004). We have described a SA model for the acceleration of  $^3\text{He}$  and  $^4\text{He}$  in SEPs by PWT assuming some characteristics for this turbulence. We have shown that for reasonable values of parameters describing the PWT and the background plasma the model gives acceptable fit to the spectra and explains the extreme enhancement of  $^3\text{He}$ . Model fits are obtained for a few events. In general relative to the loss rate  $^3\text{He}$  acceleration rate is much higher than that of  $^4\text{He}$ . All  $^3\text{He}$  particles are accelerated while only a small fraction of  $^4\text{He}$  ions attain higher energies. The primary reason for this is that the presence of a significant abundance (relative to protons) of  $\alpha$ -particles in the background plasma allows excitation of PC branch waves. It is shown that nonrelativistic  $^3\text{He}$  and  $^4\text{He}$  ions resonate mostly with waves with frequencies close to the  $\alpha$ -particle gyro-frequency. To study the SA of these ions the exact dispersion relation for the plasma waves must be used, resulting in more efficient acceleration than scattering that could lead to anisotropic particle distributions. The presence of cosmic abundance of  $\alpha$ -particles in the background plasma then play a key role in determining the relative acceleration of the two ions, because of their modification to the dispersion relation, so that low-energy  $^4\text{He}$  ions interact only with low phase velocity waves giving rise to a long acceleration time. In addition, the stronger the damping of the waves, (i.e., the lower the value of the cutoff  $k_{\text{max}}$  and/or the larger the cutoff index  $q_n$ ), the stronger the suppression of the acceleration of  $^4\text{He}$  and the higher the enhancement of  $^3\text{He}$ . On the other hand, a higher background temperature (which could cause a stronger damping) increases the efficiency of  $^4\text{He}$  acceleration up to tens of keV.

- The turbulence intensity determines the hardness of the accelerated particle spectra; Harder spectra and smaller  $^3\text{He}$  enhancements arise from stronger turbulence.

- In a strongly magnetized plasma (lower value of  $\alpha$ ) the condition becomes more favorable for acceleration of  $^4\text{He}$  and the  $^3\text{He}$  enhancement decreases. The  $\alpha$  parameter also affects the ion spectra.

- The effect of the lower wavenumber  $k_{\text{min}}$  (large scale) cutoff in the spectrum of turbulence is felt at high energies by both ions; the cutoff energy increases for lower values of  $k_{\text{min}}$ .

We note, however, that not all feature of observed spectra can be described easily by

the model. In the MeV/nucleon energy range both  $^3\text{He}$  and  $^4\text{He}$  ions interact mostly with the same waves in the PC branch, the acceleration time of  $^4\text{He}$  is always longer than that of  $^3\text{He}$ . As a result, the model predicts a  $^3\text{He}$  spectrum that is always harder than that of  $^4\text{He}$ . This is in conflict with the observed decrease of  $^3\text{He}$  to  $^4\text{He}$  ratio with energy above a few MeV/nucleon in some flares (Mason et al. 2002; Reames et al. 1997; Möbius et al. 1982; Möbius et al. 1980). This may suggest inadequacy of the simple model used here; e.g. it is possible that at high energies obliquely propagating waves becomes more important. Or this may require a special injection process or a second-phase shock acceleration (Van Hollebeke, McDonald & Meyer 1990; Serlemitsos & Balasubrahmanyam 1975; Reames et al. 1997).

In the model described here the PC branch plays a dominant role in the acceleration of  $^3\text{He}$  and  $^4\text{He}$  ions. Detailed studies of the generation of waves in this branch and a comprehensive investigation of the thermal damping effects will reduce the model parameters considerably, giving better constraints on the SA models. It is clear that the model can also be used to study the acceleration of heavy-ions. The heavy-ion acceleration is dominated by resonant interactions with waves in the HeC branch, and ions with lower charge-to-mass ratio are accelerated more efficiently due to their interactions with larger scale waves (Mason et al. 1986; Mason et al. 2004; Reames & Ng 2004). With simultaneous observations of solar flares by the *WIND* and *ACE* spacecrafts, a comprehensive study of acceleration of all charged particles including electrons, protons, and ions by the same PWT will set strict constraints on the power spectrum of PWT, guiding the exploration of the dynamical properties of the plasma turbulence. A complete time dependent treatment of the wave-particle interaction, including the coupled kinetic evolution of the particle distribution and the turbulence spectrum is also required.

This research was partially supported by NSF grant ATM-0312344, NASA grants NAG5-12111, NAG5 11918-1 at Stanford and NASA grant PC 251429 at University of Maryland.

## REFERENCES

- Bieber, J. W., Matthaeus, W. H., Smith, C. W., Wanner, W., Kallenrode, M. B., & Wibberenz, G. 1994, *ApJ*, 420, 294
- Cho, J., & Lazarian, A. 2003, *MNRAS*, 345, 325
- Cho, J., & Lazarian, A. 2004, *ApJ*, 615, L41

- Desai M. I., Mason, G. M., Dwyer, J. R., Mazur, J. E., Smith, C. W., & Skoug, R. M. 2001, ApJ, 553, L89
- Desai, M. I. et al. 2003, ApJ, 588, 1149
- Desai, M. I., et al. 2004, ApJ, 611, 1156
- Dröge, W. 2003, ApJ, 589, 1027
- Dung, R., & Petrosian, V. 1994, ApJ, 421, 550
- Fisk, L. A. 1978, ApJ, 224, 1048
- Hamilton, R. J., & Petrosian, V. 1992, ApJ, 398, 350
- Hirose, S., Krolik, J. H., De Villiers, J. P., & Hawley, J. F. 2004, ApJ, 606, 1083
- Holman, G. D. 1985, ApJ, 293, 584
- Hsieh, K. C., & Simpson, J. A. 1970, ApJ, 162, L191
- Hua, X. M., Ramaty, R., & Lingenfelter, R. E. 1989, ApJ, 341, 516
- Hurford, G. J., Mewaldt, R. A., Stone, E. C., & Vogt, R. E. 1975, ApJ, 201, L95
- Liu, S., Petrosian, V., & Mason, G. M. 2004, ApJ, 613, L81 (LPM04)
- Mason, G. M., Dwyer, J. R., & Mazur, J. E. 2000, ApJ, 545, L57
- Mason, G. M., Mazur, J. E., & Dwyer, J. R. 1999, ApJ, 525, L33
- Mason, G. M., Mazur, J. E., & Dwyer, J. R. 2002, ApJ, 565, L51
- Mason, G. M., Mazur, J. E., Dwyer, J. R., Jokipii, J. R., Gold, R. E., & Krimigis, S. M. 2004, ApJ, 606, 555
- Mason, G. M., Ng, C. K., Klecker, B., & Green, G. 1989, ApJ, 339, 529
- Mason, G. M., Reames, D. V., Klecker, B., Hovestadt, D., & von Rosenvinge, T. T. 1986, ApJ, 303, 849
- Mason et al. 2002, ApJ, 574, 1039
- Mazur, J. E., Mason, G. M., & Klecker, B. 1995, ApJ, 448, L53

- Miller, J. A. 2003, Multi-Wavelength Observations of Coronal Structure and Dynamics eds. Petrus C.H. et al. (COSPAR Colloquia Series Vol. 13), 387
- Miller, J. A., & Ramaty, D. A. 1987, Sol.Phys., 113, 195
- Miller, J. A., & Viñas, A. F. 1993, ApJ, 412, 386
- Möbius, E., Hovestadt, D., Klecker, B., & Gloeckler, G. 1980, ApJ, 238, 768
- Möbius, E., Scholer, M., Hovestadt, D., Klecker, B., & Gloeckler, G. 1982, ApJ, 259, 397
- Paesold, G., Kallenbach, R., & Benz, A. O. 2003, ApJ, 582, 495
- Park, B. T., Petrosian, V., & Schwartz, R. A. 1997, ApJ, 489, 358
- Petrosian, V., & Donaghy, T. Q. 1999, ApJ, 527, 945
- Petrosian, V., & Liu, S. 2004, ApJ, 610, 550 (PL04)
- Pryadko, J. M., & Petrosian, V. 1997, ApJ, 482, 774
- Ramaty, R. 1979, in Particle Acceleration Mechanisms in Astrophysics, eds. J. Arons, C. Max, & C. McKee (New York: AIP) 135
- Reames, D. V., Barbier, L. M., von Roseninge, T. T., Mason, G. M., Mazur, J. E., & Dwyer, J. R. 1997, ApJ, 483, 515
- Reames, D. V., Meyer, J. P., & von Roseninge, T. T. 1994, ApJS, 90, 649
- Reames, D. V., & Ng, C. K. 2004, ApJ, 610, 510
- Reames, D. V., von Roseninge, T. T., & Lin, R. P. 1985, ApJ, 292, 716
- Schlickeiser, R. 1989, ApJ, 336, 243
- Serlemitsos, A. T., & Balasubrahmanyam, V. K. 1975, ApJ, 198, 195
- Share, G. H., & Murphy, R. J. 1998, ApJ, 508, 876
- Steinacker, J., Meyer, J. P., Steinacker, A., & Reames, D. V. 1997, ApJ, 476, 403
- Swanson, D. G. 1989, Plasma Waves (Academic Press, Inc.)
- Temerin, M., & Roth, I. 1992, ApJ, 391, L105
- Van Hollebeke, M. A. I., McDonald, F. B., & Meyer, J. P. 1990, ApJ, 73, 285

- Xie, H., Ofman, L., & Viñas, A. 2004, JGR, 109, A08103
- Yan, H., Petrosian, V., & Lazarian, A. 2005, in preparation.
- Zhang, T. X. 1999, ApJ, 518, 954